High-resolution modeling of sediment erosion and particle transport across the northwest African shelf

G. Karakaş,[1] N. Nowald,[2] M. Blaas,[3] P. Marchesiello,[4] S. Frickenhaus,[1] and R. Schlitzer[1]

Received 16 September 2005; revised 15 December 2005; accepted 23 February 2006; published 17 June 2006.

[1] The region off Cape Blanc along the northwest African coast is dominated by persistent upwelling and strong activity of small-scale eddies, filaments, and jets. Vertical particle camera profiles obtained during recent cruises in this region show that there exist two well-marked maxima of particle abundance in the water column, one at the surface and the other in subsurface layers between 200 m and 400 m depths. Using a high-resolution (2.7 km) terrain-following coordinate ocean model with built-in ecosystem and sediment transport modules, we show that the surface particle maximum can be explained by local productivity, while the deeper, subsurface particle cloud most likely originates from particulate material eroded from the shallow shelf and transported offshore by vigorous filament activity and dynamic features of the flow. In the numerical experiments, particles are produced either by primary production in the surface layer or from prescribed sediment sources to mimic suspension and erosion along the shelf areas. Good agreement of modeled particle distributions with the data is achieved with a typical settling velocity of 5 m day^{-1}. Time-averaged effective transport patterns of particles reveal distinct maxima between 20.5°N and 23.5°N off Cape Blanc. In the south of Cape Bojador and off Cape Timiris, on the other hand, the effective transport distance patterns suggest energetic offshore activity.

Citation: Karakaş, G., N. Nowald, M. Blaas, P. Marchesiello, S. Frickenhaus, and R. Schlitzer (2006), High-resolution modeling of sediment erosion and particle transport across the northwest African shelf, *J. Geophys. Res.*, *111*, C06025, doi:10.1029/2005JC003296.

1. Introduction

[2] Coastal regions emerge as important players of the global carbon cycle despite their relatively small surface area in the world ocean. They are characterized not only by high primary productivity but also by high downward flux of particulate matter, making them a potentially large sink for CO_2. *Muller-Karger et al.* [2005] argue that the oceanic biological pump sequesters 40% of the carbon on continental margins. Besides, the margins serve as a source of organic matter to the deep ocean. Transport of organic carbon from the upper slope and shelf regions to the open ocean in dissolved and suspended particulate forms are suggested to be more than an order of magnitude greater than organic carbon inputs from the surface ocean [*Bauer and Druffel*, 1998].

[3] The NW African coastal zone is one of the major upwelling regions of the world ocean [*Wooster and Reid*, 1963] and exhibits high rates of primary productivity [*Behrenfeld and Falkowski*, 1997; *Davenport et al.*, 2002], high export fluxes of particulate organic carbon [*Schlitzer*, 2000] and high organic carbon deposition in the sediments [*Muller-Karger et al.*, 2005; *Jahnke*, 1996]. Satellite images of sea surface temperature and chlorophyll reveal intense and highly variable jets, filaments and eddies in the area [*Van Camp et al.*, 1991; *Nykjær and Van Camp*, 1994; *Kostianoy and Zatsepin*, 1996]. These mesoscale dynamics affect the regional nutrient and carbon budgets and modify the high productivity in the coastal transition zone through turbulent mixing processes between nutrient rich coastal and poor offshore waters [*Marchesiello et al.*, 2004]. The intense and highly variable currents also lead to a resuspension and redistribution of the shallow shelf sediments and to a net offshore transport of particulate material.

[4] Various authors report the strong influence of filament activity off NW Africa on the patterns of matter dispersion and its offshore transport [*Barton et al.*, 1998; *Arístegui et al.*, 2004; *García-Muñoz et al.*, 2004; *García-Muñoz et al.*, 2005; *Pelegrí et al.*, 2005]. This has significant implications, in particular, in the area off Cape Blanc, between 20°N and 25°N, where persistent upwelling is reported year round [*Gabric et al.*, 1993]. Cape Blanc is therefore a major spot along the NW Africa for the offshore advection of particles. Upwelling at this site shows its maximum intensity in spring and autumn. North of 25°N and south of 20°N, however, it has seasonal dependency and is mainly confined to summer and autumn, and winter respectively [*Mittelstaedt*, 1991; *Nykjær and Van Camp*, 1994].

[1] Alfred Wegener Institute for Polar and Marine Research, Bremerhaven, Germany.
[2] Department of Geosciences, University of Bremen, Bremen, Germany.
[3] WL|Delft Hydraulics, Delft, Netherlands.
[4] Institut de Recherche pour le Développement, Plouzane, France.

0148-0227/06/2005JC003296

[5] Main components of the large scale surface circulation in the Cape Blanc region are the Canary Current, which detaches from the continental slope between 21°N and 25°N, flows southwest to feed the North Equatorial Current, and eventually forms the southern boundary of the subtropical gyre, and a persistent mesoscale cyclonic gyre south of Cape Blanc, which moves seasonally. This gyre is an extension of the northern branch of the North Equatorial Counter Current [*Mittelstaedt*, 1991; *Richardson et al.*, 1992; *Stramma and Schott*, 1999]. Because the region is a frontal zone between relatively cold North Atlantic Central Water (NACW) and warmer, less saline South Atlantic Central Water (SACW), the circulation is influenced by the thermohaline mixing processes and pertains a complex mesoscale regime [*Barton*, 1987; *Barton*, 1998].

[6] A variety of interacting physical and biogeochemical processes determine the extent of particle fluxes across the NW African shelf. Upwelling along the NW African coast is a wind-driven process. Alongshore winds lead to coastal divergence and offshore Ekman transport of surface waters, which is offset by upwelling of nutrient-rich deeper waters to the surface, where these waters stimulate biological production. Offshore transport of surface waters carry nutrients and particulate matter away from the coastal area, which results in the offshore deposition of biogenic and lithogenic particles. Aggregation and disaggregation processes affect the settling velocities of the particles, the particle distributions in the water column and the deposition patterns in the sediment. The region off NW Africa is characterized by the largest dust deposition rates worldwide [*Mahowald et al.*, 1999; *Jickells et al.*, 2005] and lithogenic particles arising from dust deposition serve as ballast for the fast removal of settling particles from surface layers [*Armstrong et al.*, 2002]. The sinking lithogenic particles are often found in sediment traps located in coastal or deep ocean waters [*Ratmeyer et al.*, 1999].

[7] Most studies related to the transport of particulate matter in the region rely on the analysis of satellite imagery of ocean color and examination of cruise data or recordings of sediment trap deployments. While some workers give estimations of primary productivity by making use of the images from the Coastal Zone Color Scanner (CZCS) [*Bricaud et al.*, 1987; *Dupouy and Demarcq*, 1987; *Gabric et al.*, 1993] or the Sea-viewing Wide Field-of-view Sensor (SeaWiFS) [*Davenport et al.*, 2002], others describe the significance of eddies and filaments in offshore transport of organic matter in the northern part of the region, mostly around the Canaries [*Van Camp et al.*, 1991; *Hernández-Guerra et al. 1993*: *Arístegui et al.*, 1997]. Upwelling filaments are also shown to be the most probable process responsible for the sedimentation peaks seen in the sediment traps [*Davenport et al.*, 1999].

[8] However, some authors report a restricted transport capacity of filaments. Studying the data obtained during a cruise in August 1999, *Arístegui et al.* [2004] show that the Cape Juby filament in the north has lower sedimentation rates of particulate organic carbon compared to other filament studies in the NE Atlantic coast. This is caused by the recirculation of the filament water by an associated cyclonic eddy, which traps the organic matter. *García-Muñoz et al.* [2004, 2005], on the other hand, investigate the Cape Ghir and the Cape Juby-Cape Bojador filament systems and report a large amount of organic matter transport even in the absence of upwelling favorable conditions.

[9] Sediment traps have often been used in the region and various properties of the records collected have been analyzed. *Lange et al.* [1998], for instance, examining diatom and silicoflagellate fluxes off Cape Blanc, report a strong seasonality in diatom fluxes with increased rates during upwelling, although no seasonality was marked with the fluxes of silicoflagellate. Similarly, *Neuer et al.* [2002] investigate the seasonal and depth variation of particle fluxes along an east-west transect in the Canary Islands region and points out the difficulty of determining the contributory processes on the flux variability. On the basis of the records from several sediment traps at different water depths in the Canary Islands region, off Cape Blanc and off Cape Verde, *Ratmeyer et al.* [1999] suggest a relatively fast and undisturbed downward transport of particles at Cape Blanc site and show that this site records the highest annual mean lithogenic fluxes, but also the weakest seasonality.

[10] Recent observations by N. Nowald et al. (Distribution and transportation processes of marine particulate matter off Cape Blanc (NW-Africa): Results from high resolution, vertical camera profiles, submitted to *Journal of Geophysical Research*, 2006, hereinafter referred to as Nowald et al., submitted manuscript, 2006) using a deep-sea particle camera system recorded vertical particle profiles at several locations off Cape Blanc in spring months of 3 consecutive years. The profiles show pronounced particle abundance maxima both at the surface and in subsurface layers between 200 m and 400 m depths. The authors also report an increased frequency of large particles toward the bottom and suggest a downslope movement of particles along the seafloor.

[11] Because the temporal and spatial extent of deployment sites are limited, sediment traps and in situ measurements of particle concentrations reveal very little clue as to the origin or the destination of particles. Particularly problematic are the dynamic upwelling systems like NW African coast, where flow features on submesoscales play an important role in the distribution of biogeochemical properties. Numerical modeling can help to gain a comprehensive picture of the processes involved and enhance our understanding of the complexity of the system by analyzing the interaction of these processes with one another. This is best done with an idealized approach, in which the effects of different processes are studied individually.

[12] In order to resolve eddies and offshore filament flow to a sufficient degree, in this study we used a high-resolution, terrain-following coordinate ocean model for the region off NW Africa with built-in sediment transport and ecosystem modules in a nested configuration. The small grid is zoomed in off Cape Blanc, where upwelling is most intense. We test two hypotheses by conducting numerical experiments in an attempt to investigate the possible sources of high particle abundance seen in the subsurface layers in Cape Blanc region as the vertical camera profiles indicate (Nowald et al., submitted manuscript, 2006). Our aim is to examine and find out whether these particle maxima might be due to primary production or shelf erosion, which are considered as two hypothetical particle sources. We observe

the simulated subsequent distribution patterns of the particles after their production and release.

2. Model

[13] The model employed herein is the Regional Ocean Modeling System, ROMS [*Shchepetkin and McWilliams*, 2005]. ROMS is a hydrostatic, free-surface, primitive-equation ocean model with curvilinear coordinates in the horizontal on an Arakawa C-grid and has been developed for a realistic simulation of the interactions between the coastal regions and open ocean, making it an appropriate tool for our application.

[14] Dynamic features of the region off NW Africa are set through the interplay of alongshore Canary Current, topography, upwelling, and offshore filaments, and therefore the most critical expectation from an ocean model to use in this application is an ability to handle the dynamic processes both in shelf and open ocean regions without compromising numerical stability. In fact, the choice of the vertical coordinate system has been the most essential aspect of an ocean model's design in terms of parameterization. The performance of ocean models with different vertical coordinates is not optimal everywhere but varies from one place to the other in the ocean as shown by the recent model comparison exercises [*Chassignet and Malanotte-Rizzoli*, 2000; *Chassignet et al.*, 2000; *Meincke et al.*, 2001]. While isopycnic coordinates seem to produce the most satisfactory results in the stratified open ocean, z-level depth cordinates could maintain high vertical resolution in unstratified or weakly stratified regions of the ocean, and terrain-following coordinates achieve high vertical resolution in shallow, coastal regions with better representation of the interactions between the topography and ocean dynamics. The disadvantage of terrain-following models is a stronger sensitivity to topography when stretching them over the continental slope to the open ocean. This inherits pressure gradient errors, which arise due to splitting of the pressure gradient term into an along-sigma component and a hydrostatic correction [*Haidvogel and Beckmann*, 1999]. ROMS, on the other hand, appeared to tackle the problems associated with the terrain-following coordinates. Pressure gradient algorithms in ROMS have been improved significantly and mechanisms have been worked out to smooth topography within the limits of validity [*Shchepetkin and McWilliams*, 2003].

[15] Terrain-following stretched coordinates of ROMS in the vertical allow enhanced resolution at the sea surface or sea floor. Besides, the model adopts a mode splitting technique for computational economy, which enables the separation of the barotropic and baroclinic components in the model with internal and external time steps. The specially designed predictor-corrector time step algorithm brings about a substantial increase in the permissible time-step size. The ROMS code has been designed for shared-memory computer architectures and provides an explicit two dimensional partitioning of the model domain into subdomains for paralellization and optimal use of processor caches, which encourages high-resolution setups. Furthermore, the model offers a numerically stable open boundary treatment with the ability to enforce volume conservation. It employs a dynamic combination of outward radiation and flow-adapted nudging towards prescribed external conditions. ROMS has been successfully applied and validated for the California upwelling system [*Marchesiello et al.*, 2003]. The reader is referred to *Shchepetkin and McWilliams* [2003, 2005] and *Marchesiello et al.* [2001] for the details of the model numerics and its open boundary treatment, respectively.

[16] We exploit the nesting capability of ROMS, which allows embedded subdomains with higher resolution in a larger parent domain of coarser resolution [*Penven et al.*, 2006]. Nesting therefore makes investigating the local processes at high resolutions possible without isolating them from the influence of larger-scale dynamics. In embedded domains lateral boundary conditions for the fine grid are supplied by the coarse grid solution. Nesting in ROMS is achieved by the AGRIF (Adaptive Grid Refinement in Fortran) package [*Blayo and Debreu*, 1999]. AGRIF applies adaptive mesh refinement features in a finite difference model, based on the use of pointers, and minimizes the need for changes in the original code. Temporal coupling between the parent and child grids in the model, which is done at each baroclinic time step, is controlled by a recursive integration procedure. The CFL criterion is preserved by advancing the child time step as many times as the coefficient of refinement to reach the parent time step. Then, the relevant parent variables in space and time are interpolated to get the boundary conditions for the child grid.

2.1. Ecosystem Model

[17] The ecosystem model in ROMS is a modified version of Fasham's model [*Fasham et al.*, 1990] adapted for upwelling systems (N. Gruber et al., Simulation of phytoplankton ecosystem dynamics in the California Current System, submitted to *Deep-Sea Research*, 2006, hereinafter referred to as Gruber et al., submitted manuscript, 2006). The model consists of a four compartment nitrogen based N-P-Z-D type model in a series of steps within the main food chain. The growth rate of phytoplankton is determined by available photosynthetically active radiation and the concentration of nitrate. Surface chlorophyll is not a prognostic variable but calculated from the model state. The phytoplankton compartment also involves the grazing of zooplankton on phytoplankton and the mortality of phytoplankton. The zooplankton compartment includes processes of zooplankton growth, excretion to nitrate, and mortality to detritus. The detritus compartment is fed by a fraction from the phytoplankton and zooplankton as a result of grazing and mortality and is partly lost to sinking and remineralization. The nitrogen compartment in turn receives nitrate from remineralization and due to excretion and is consumed by the phytoplankton growth. Open boundary treatment of the model handles biology components in the same way as other tracers. We refer interested reader to Gruber et al. (submitted manuscript, 2006) for the details of the ecosystem model.

2.2. Sediment Transport Model

[18] Sediment transport is an integral part of ROMS [*Blaas et al.*, 2006]. Since in this paper we treat all sediment fractions as noncohesive (aggregation and dissociation are deferred to later studies), the suspended sediment concen-

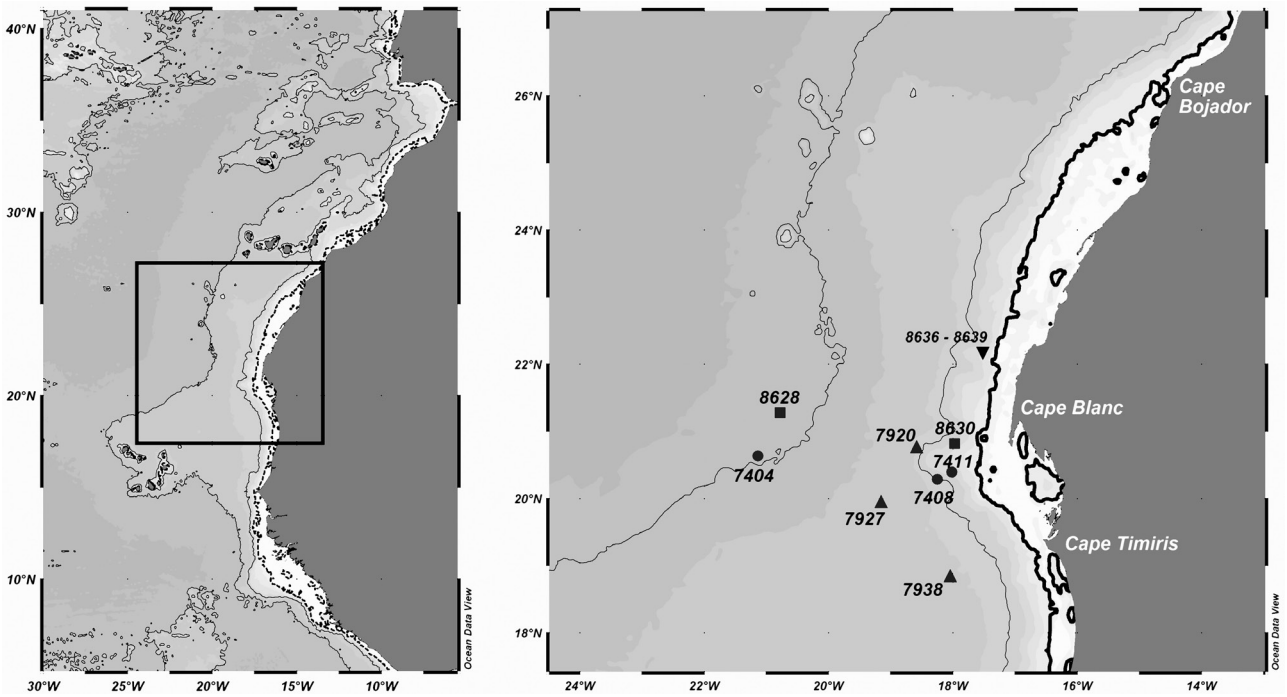

Figure 1. Model topography for the parent (left) and child grid (right). The model consists of two nested grids; the child grid of 2.7 km resolution is located off Cape Blanc region and embedded within a parent grid of 8km resolution. Contour lines for 4000 m and 2000 m bathymetry are shown. The dashed lines indicate the 135 m depth contour, i.e., the maximum release depth of particles in the shelf erosion experiment. Positions of profiling stations of the particle camera during Poseidon 272, 2001 (circle), Meteor 53-1, 2002 (triangle), and Meteor 58-2b, 2003 (square) cruises are also shown.

tration equation is solved independently for each particle size class j. The concentration equation is a modification of the general advection-diffusion equation for tracers in ROMS:

$$\frac{\partial c_j}{\partial t} + \frac{\partial u_i c_j}{\partial x_i} - \frac{\partial}{\partial x_i}\left(K_i \frac{\partial c_j}{\partial x_i}\right) - w_{sj}\frac{\partial c_j}{\partial x_3} = Q_j. \quad (1)$$

Here c_j is the noncohesive suspended sediment concentration of size class j. Subscripts i (using index summation convention) denote direction (x_3 vertically upward); u_i is velocity; K_i is eddy diffusivity; w_{sj} is the settling velocity; and Q_j represents internal sources and sinks.

[19] Horizontal diffusion of sediments is not explicitly solved for ($K_1 = K_2 = 0$ m^2 s^{-1}) since the advection scheme by *Shchepetkin and McWilliams* [1998] makes use of a locally adaptive, dissipative operator. Vertical eddy diffusivity for tracers (K_3, further denoted as K_v) is determined using the K-Profile Parameterization (KPP) by *Large et al.* [1994]. This scheme includes surface and bottom boundary layer parameterizations. The vertical settling scheme is not constrained by the CFL criterion so that also relatively fast vertical settling velocities can be handled correctly even over shallow topographies. A more detailed description of the sediment transport model in ROMS, including erosion, armoring and sediment bed formulations, is provided by *Blaas et al.* [2006].

2.3. Model Configuration and Numerical Experiments

[20] In the present configuration a model domain with 2-level embedding is constructed. The parent domain covers the area from 5°N to 41°N and from 30°W to 5.5°W with a resolution of approximately 8 km. The embedded grid is located on the region off Cape Blanc as shown in Figure 1, and extends between 17°N–28°N and 13°W–24°W at a resolution of 2.7 km. With this resolution we expect to resolve the dynamic temporal and spatial variability of the flow regime associated with submesosclale features in the region, manifested as dipole eddies, squirts, and filaments in the satellite imagery of surface temperature or chlorophyll distribution. Vertically, 32 levels are described on s-coordinates with an increasing refinement near the surface. The topography of the model is obtained from the ETOPO2 analysis [*Smith and Sandwell*, 1997] and is slightly smoothed to ensure stable numerical solutions [*Haidvogel et al.*, 2000] (see Figure 1). The shelf width in the embedded grid varies from 30km off Cape Bojador, Cape Blanc, and Cape Timiris to more than 100km in between these capes.

[21] Monthly averaged data from COADS (Comprehensive Ocean-Atmosphere Data Set) are employed to force the model for the heat, fresh water and momentum fluxes [*da Silva et al.*, 1994]. The model is initially at rest with the January climatology of World Ocean Atlas 2001 (WOA2001) [*Stephens et al.*, 2002; *Boyer et al.*, 2002]. Monthly means of this climatology are also used for the prescription of temperature, salinity, and momentum fluxes along the three lateral open boundaries where an implicit active radiative scheme is adopted [*Marchesiello et al.*, 2001]. The scheme enables nudging toward climatological values when the flux is directed inward. Besides, sponge layers at a width of 150 km are defined along the bound-

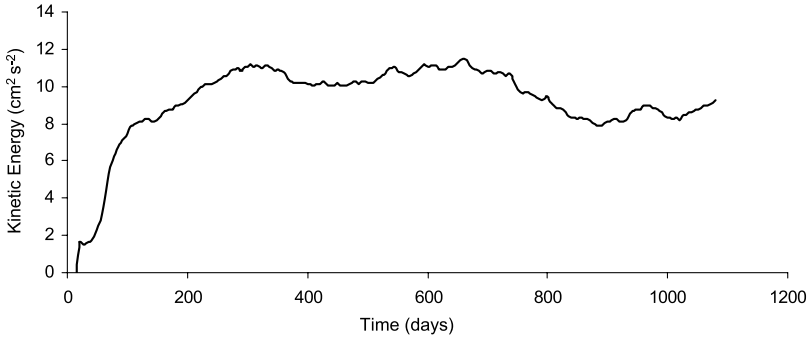

Figure 2. Volume averaged kinetic energy ($cm^2\ s^{-2}$) for the parent grid.

aries. The Mediterranean outflow is parameterized by nudging temperature and salinity for depths deeper than 750 m to their monthly WOA2001 means with a timescale of 50 days.

[22] In the first experiment, we used the ecosystem model in ROMS to examine our first hypothesis, if the biological particle production contributes to the high particle abundance seen in the vertical camera profiles. WOA2001 climatology of NO_3, chlorophyll, and phytoplankton is used for the initialization of the ecosystem model and relaxation along the lateral boundaries. Settling velocity of detritus is typically specified as 5 m day^{-1} and it is worth noting that this value is far smaller than the estimated sinking velocity of large particles captured in sediment traps in the region (100–200 m day^{-1}) [*Wefer and Fischer*, 1993] (see section 4).

[23] In order to test the second hypothesis, that is whether the subsurface maxima in the vertical profiles observed off Cape Blanc are produced by the particles eroded along the shelf, we employ the sediment transport module. Resuspension and erosion have been effectively switched off in these simulations and explicit source terms for suspended particles have been implemented for the bottommost layers over the shallow shelf area. The sediment is therefore considered to originate from this prescribed internal source. This approach provides full control over the origins of the suspended material. The bottommost three layers of the shelf along the coastline, which have a thickness of approximately 15 m, are seeded with two fractions of particles having different settling velocities, 5 m day^{-1} and 17 m day^{-1}. Hereinafter, we refer to these particles as Class A and Class B, respectively. Maximum release depth of particles is defined as 135 m (see the dashed lines in Figure 1), that is a typical shelf break and the rate at which they are released is specified as 1000 mg l^{-1} day^{-1}. With this particular configuration we aim to portray the offshore distribution patterns of suspended particles originating from the shelf regions only by intense upwelling and offshore filament flows.

[24] Lateral open boundaries are dealt with as for any other tracer in ROMS according to the methods by *Marchesiello et al.* [2001]: on outflow radiation and advection conditions, on inflow concentrations are nudged to an external value. Because the concentrations decrease offshore and the boundaries are located far from the source regions, the nudging was to zero concentrations in our experiments.

3. Results

[25] The model was spun up for 2 years before the particle experiments were initiated. After 1 year it reaches statistical equilibrium as indicated by the volume-averaged kinetic energy shown in Figure 2. The ecosystem model has then been run for 2 additional years and we present the results from its second year. The shelf erosion experiment, on the other hand, has been run for 1 year.

3.1. General Description of Surface Dynamics

[26] In Figure 3 we compare the model SST from a snapshot in November of the third model year with a measured SST map from the NASA Moderate Resolution Imaging Spectroradiometer (MODIS) sensor for 21 November 2004. We observe that despite climatological forcing the simulations capture dynamic coastal activity of mesocale flow reasonably well (see Figure 3). The satellite SST data are processed by the Modis Adaptive Processing System (MODAPS) and available globally at 4 km resolution with daily time intervals. The SST is derived from the thermal far infrared band of MODIS channel 31 and has an accuracy of 0.3°C. The data are distributed by the Goddard Distributed Active Archive Center (GDAAC) and accessible via anonymous FTP to ftp://podaac.jpl.nasa.gov/pub/sea_ surface_ temperature/modis/data/aqua/L3_mapped/sst/. Sea surface temperature shows indications not only of upwelling and longshore flow of the Canary Current but also a northward extension of warm North Equatorial Counter Current. The simulation estimates for the upwelling intensity, that is the temperature difference between the coastal waters and the offshore waters, upwelling location as well as warm water intrusion south of Cape Timiris are generally in a good agreement with the satellite imagery and the slight discrepancies are attributed to the mean climatological forcing of the model. In Figure 4 we show surface velocities superimposed on sea surface temperature in mid-May. The cold filaments of upwelled waters and onshore intrusion of warm waters are noticeable. Offshore flow of narrow, meandering filaments between warm-core anticyclonic and cold-core cyclonic eddies, confluence of Canary Current and North Equatorial Counter Current waters off Cape Blanc and their westward flow and two cyclonic gyres on

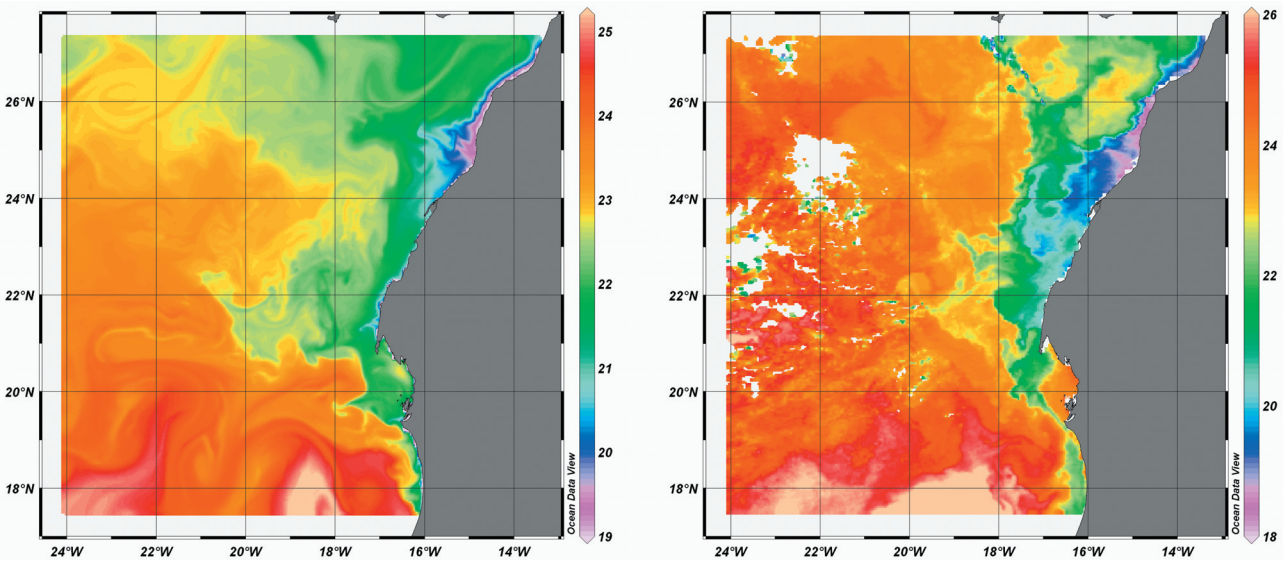

Figure 3. A snapshot of SST (°C) in November from the simulation (left) and a measured SST map from the MODIS on board the Aqua spacecraft on 21 November 2004 (right).

the south of Cape Timiris appear to be the most distinguishing features of the surface circulation.

3.2. Vertical Distributions of Detritus and Class A Type Particles in Profiling Stations

[27] Figure 5 presents the simulated vertical profiles of detritus in late April and early May, (i.e., the same period when camera profiles were measured) and 3-month mean concentrations of Class A type particles. Also shown are the particle camera profiles of particulate matter at the same stations (Nowald et al., submitted manuscript, 2006) (see Figure 1b for the location of profiling stations). It is found that the abundance of biologically produced particles (blue lines) is high in the surface layer and decreases rapidly with depth. In 250 m depth the detritus concentrations are small for all stations. The observed high surface abundance of particles seen in the camera profiles (black lines) appears to be of biological origin since very high amounts of detritus appear also at the surface in the model. However, the concentrations decrease steeply in the deeper layers and exhibit no evidence of a subsurface maxima, suggesting that subsurface particle maxima seen in the camera profiles cannot be explained by biological activity alone.

[28] The simulated vertical distributions of Class A type particles eroded from the shelf (red lines), on the other hand, do not only distinctly show the subsurface maxima at the profiling stations but they also help to explain other features seen in the camera profiles. Class A type particles in the model attain their maxima between 200 to 500 m depths in the profiling stations. The depth of the maxima appears to vary depending on the proximity to the shelf, with stations near the shelf experiencing high concentrations in shallower depths in comparison to those far from the shelf having their maxima in deeper layers. This general deepening of the particle abundance maxima with distance from the shelf can be explained by the settling of particles. The modeled thickness of high-concentration plumes can be as much as 400m (see the particle profile at station GeoB 7411). Stations close to the shelf (see the profiles at stations GeoB 7408, 7411, and 8630) show pronounced increases in particle abundance near the ocean floor in addition to the particle maxima between 200 m and 500 m depth.

[29] Comparison of the high resolution camera profiles of particle abundance with the modeled profiles of Class A type particles shows that the modeled distribution of par-

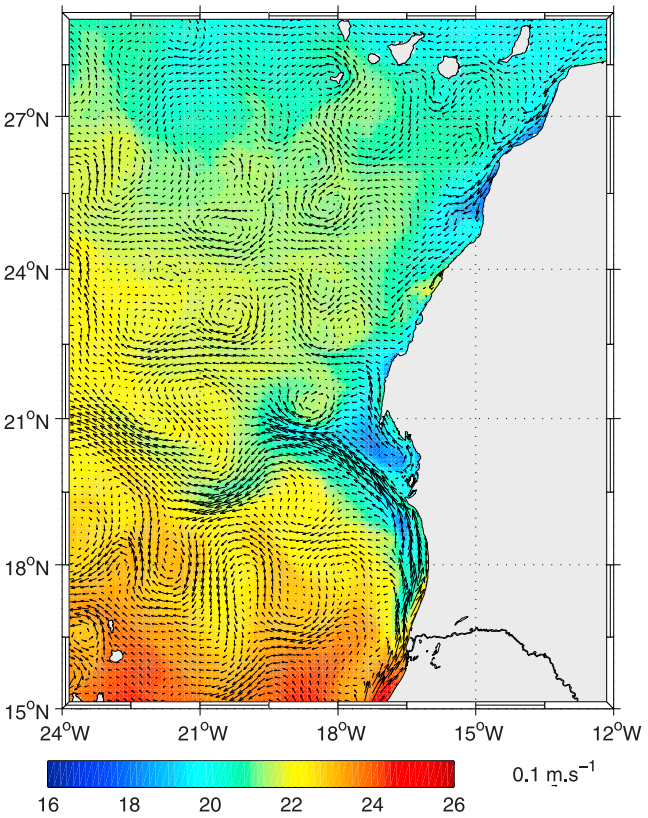

Figure 4. Surface velocity superimposed on sea surface temperature (°C) in mid-May (every second point of the parent grid is shown).

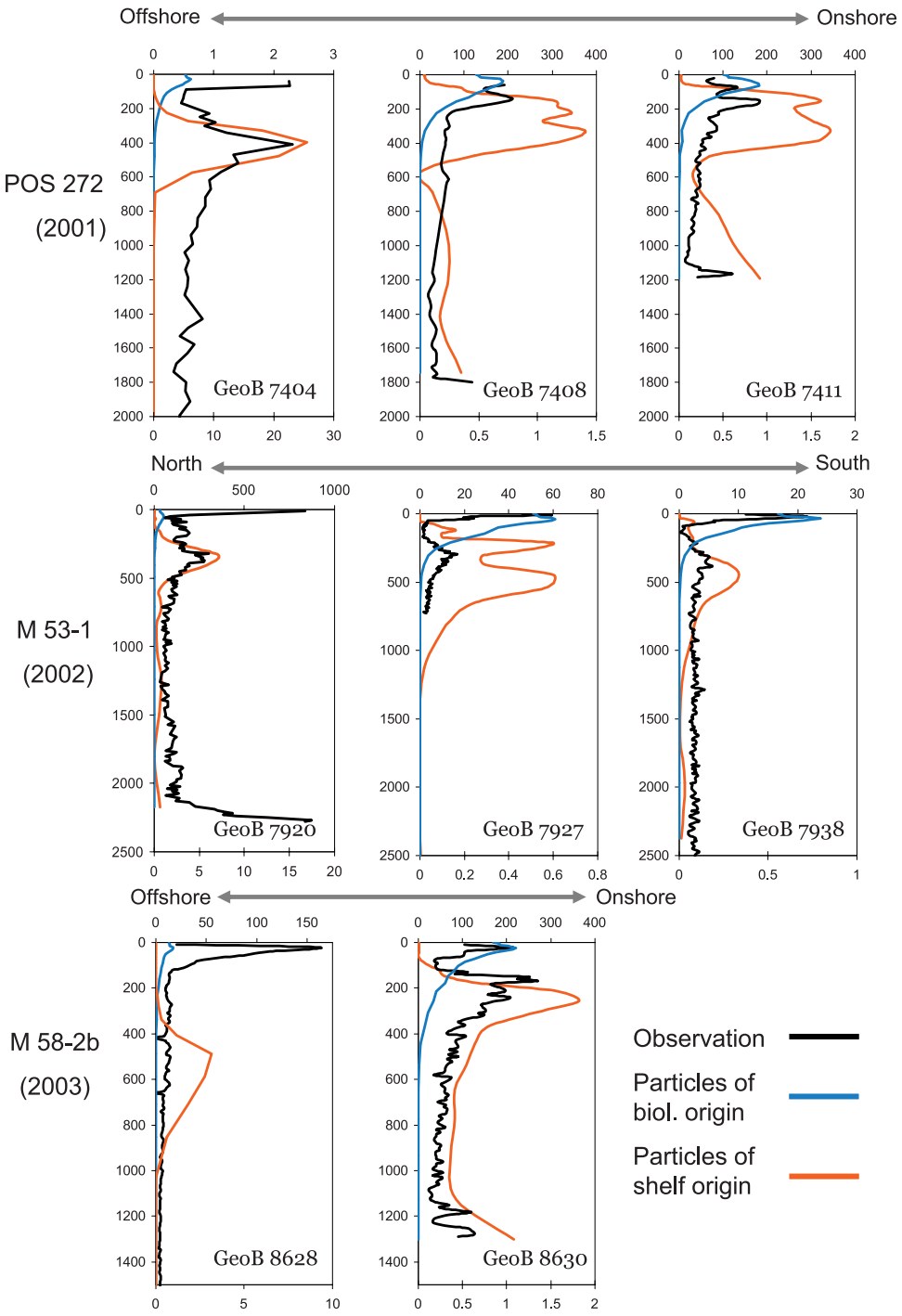

Figure 5. Vertical profiles of biologically produced particles (snapshots, blue lines, detritus in mMol N m^{-3}, top axis in GeoB 7404, bottom axis in the rest) and Class A particles (3-month averaged, red lines, relative units, bottom axis in GeoB 8628, top axis in the rest) against observed particle profiles (black lines, number per liter, bottom axis in GeoB 7404 and GeoB 7920, top axis in the rest) in spring months at the profiling stations (positions are shown in Figure 1).

ticles eroded from the shelf agree well with the particle clouds seen in the camera observations. Similar to the model Class A particles, the camera data off Cape Blanc during Poseidon 272 cruise show that particle abundance decreases in offshore direction, while the depth of their subsurface maxima increases (black lines in stations GeoB 7411, 7408, and 7404). During Meteor 53-1 cruise, on the other hand, where profiling stations are located almost alongshore (stations GeoB 7920, 7927, and 7938), subsurface maxima are found in similar depths, which also agrees with the model simulations. Moreover, measurements show an increase in particle concentrations towards ocean floor at

several stations, in agreement with the model results due to the resuspension and downslope transport of particles.

3.3. Horizontal Distribution of Class A Particles

[30] In Figure 6 we show two snapshots of horizontal particle distribution at 500 m depth taken from different days of the model simulation. Particles are transported with a patchy and irregular pattern, forming offshore intrusions at varying concentrations. Dynamic coastal activity of filaments serve as a jet for cross shore particle transfer and produces sporadic particle clouds pumped to the open ocean.

[31] It appears therefore that filaments and squirts play a dominant role in determining the pathways and fluxes of particles across the shelf. The implication of such a transport system is significant in that particles caught by an offshore filament can be transported far away from the shore within a relatively short period of time (typically around 100 km per month offshore in our simulations). The chances of observing a particle cloud during a cruise also depend on whether the profiling station is located on the route of a filament or not (see the observed particle abundance in profiling station GeoB 8628 in Figure 5, which does not indicate a subsurface particle cloud).

[32] Figure 7 illustrates the effective transport distance of Class A particles calculated from 1-year average of the simulation as defined by the offshore distance for a one or two orders of magnitude reduction in particle concentrations, i.e., the distance at which maximum particle concentrations in the water column reaches 10% (1-log) and 1% (2-log) of their value at the shore, respectively. The 1-log distribution illustrates that near Cape Blanc between 20.5°N and 23.5°N the offshore transport of particles exceeds 100 km and particularly at 22.5°N, where the Canary Current separates from the coast, it reaches up to 150 km. This suggests that near shore dynamics is stronger off Cape Blanc. The 2-log distribution gives a different zonal pattern with effective distances of up to 500 km and 600 km in the south of Cape Bojador and off Cape Timiris, respectively, which indicates more intense offshore activity in these regions.

3.4. Transport of Particles Across the Shelf

[33] Snapshots of Class A and Class B particle concentrations along a zonal transect at 21.2°N are shown in Figure 8. It is observed that Class A particles are spread in subsurface layers in the form of intermittent injections from the shelf into the open ocean (top figure). The offshore extension of these relatively slow sinking particles (5 m day^{-1}) is clearly pronounced and points out that shelf erosion in Cape Blanc site can have a significant contribution to the subsurface peaks of particle abundance rates observed in optical measurements by Nowald et al. (submitted manuscript, 2006). The dispersion pattern of Class B particles (with sinking velocity of 17 m day^{-1}) on the other hand, appears to be restricted to the bottom layers as they follow bottom slope (see the bottom figure). Although the upwelling velocities in simulations can occasionally be as high as 20 m day^{-1}, especially in Cape Bojador and Cape Blanc regions, typically they are around 8 m day^{-1}. The strength of upwelling and offshore currents therefore cannot overcome the relatively fast sinking rates of these particles and confine bulk of them to the bottom layers where they are originally released. Migrating downslope appears to be the major cross-shelf transport mechanism for the Class B particles that are suspended in the water column. This argument is also supported by Nowald et al. (submitted manuscript, 2006) who report increased abundance rates and larger particle sizes toward the ocean floor.

[34] In Figure 9 we show four profiles obtained overnight during the Meteor cruise 58-2B in 2003 along 22.15°N, a cross shore transect slightly north of Cape Blanc. Vertical distribution of simulated Class B particles is also plotted. Camera profiles demonstrate a distinct increase in the number of particles toward the sea floor along this slope area and give indications of a downslope particle movement. Although resuspension is effectively switched off in the model, the concentration of Class B particles also grows, which points to the transport of freshly input particles from the shelf into the slope by strong filament flow or alongshore currents.

4. Discussion

[35] The simulations indicate that particulate matter suspended on the shelf is subjected to either downslope transport (Class B particles) or advected seaward as intermittent shelf-edge plumes after detaching from the shelf or upper slope (Class A particles). This continuous transport of particulate matter from the shelf leads to their restricted net accumulation on the shelf. Looking at the textural and compositional analysis of the surface sediments off NW Africa between 13°N and 26°N, *Fütterer* [1983] shows that the onshore-offshore and alongshore compensation currents prevent deposition of fine-grained material on the shelf and that most of the upwelling-derived material is transported beyond the shelf edge into open ocean areas. Off Cape Blanc, he indicates the midslope below 1000 m as the final destination where the accumulation occurs. In fact, *De Haas et al.* [2002], after giving an account of various shelf regions as potential sinks for organic carbon, conclude that only locally and rarely large amounts of carbon are deposited on the shelf and that present day shelf seas do not play an important role in the burial of organic carbon. The great part of organic carbon that escapes mineralization in shelf regions is transported over the shelf edge and deposited on the slope or further seaward. *Wheatcroft et al.* [1997] show that more than half of the Eel River's annual sediment input does not remain on the nearby shelf on the northern California margin. Similarly, for the upper northwest Iberian margin, where wind-driven upwelling is seasonal, *van Weering et al.* [2002] report little net accumulation of depositing matter after studying five transects during Ocean Margin Exchange II project. Other authors point out that at the NW European continental margin, horizontal, advective fluxes of particulate matter exceed the vertically sinking fluxes through the water column several orders of magnitude even under low flow conditions [*Thomsen and van Weering*, 1998; *Thomsen et al.*, 2002]. Drift estimates at this margin suggest that significant sediment accumulation on the lower slope is due to downslope transport in the benthic boundary layer [*McCave et al.*, 2001]. Even on the shelf off Somalia-Yemen-Oman, where high rates of organic carbon accumulation are expected due to upwelling, peak concen-

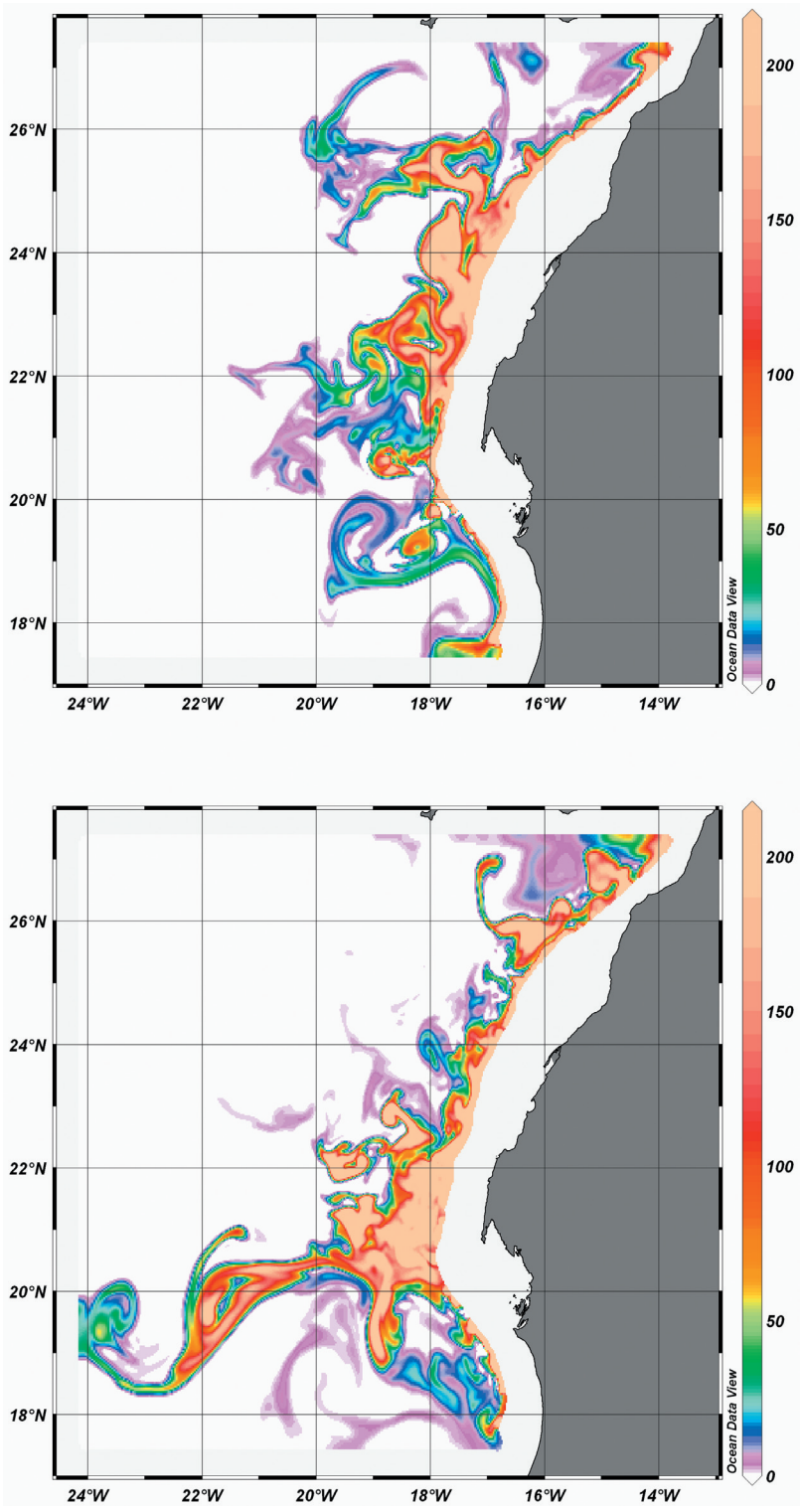

Figure 6. Snapshots of horizontal distribution of Class A particles (concentrations in relative units) at 500 m depth on days 935 (top) and 1035 (bottom) of the simulation.

trations are found on the upper slope [*Paropkari et al.*, 1992] because of the matter transport by strong currents. Eventually organic matter is further carried from the slope into the deep sea [*van Weering et al.*, 1997].

[36] We note that because particles in our simulations are continuously seeded into the water column, subsurface maxima of Class A particles are seen in all profiling stations in the model results. However, in reality the suspension follows upwelling, which is an intermittent event due to varying wind forcing. Therefore camera measurements do not always show a maximum. This is

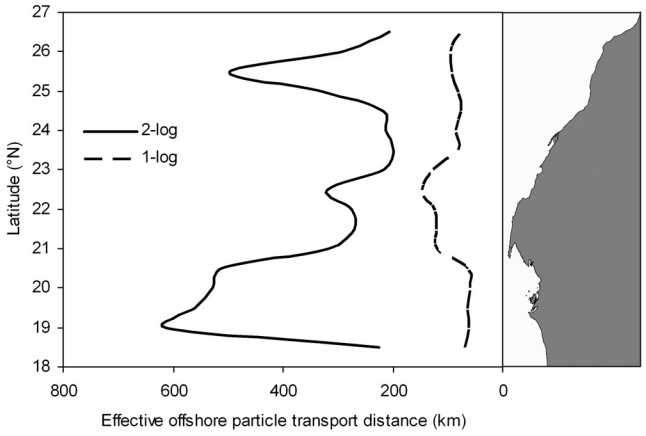

Figure 7. Effective transport distance of Class A particles given by the offshore distance prior to a 1-log and 2-log reduction in particle concentrations (i.e., the distance at which maximum particle concentrations in the water column reaches 10% and 1% of their value at the shore, respectively).

the case in profiling station GeoB8628 or in other stations which are shown in Figure 9.

[37] The detachment of suspended particle clouds from the shelf or upper slope and their seaward extension as observed in the simulations are not uncommon along continental margins and have often been referred as Intermediate Nepheloid Layers (INLs) [*Dickson and McCave*, 1986; *Hall et al.*, 2000; *Frignani et al.*, 2002; *van Weering et al.*, 2002]. It is demonstrated that horizontal, offshore matter transport with INLs contribute more to eventual deposition on the outer slope than the vertical settling of surface material [*van Weering et al.*, 1997; *McPhee-Shaw et al.*, 2004]. Typically, benthic nepheloid layers (BNLs) generate INLs as they are advected off the shelf as a shelf-edge plume. *Dickson and McCave* [1986] report intensification of bottom water movements and internal waves for the generation of INLs through upwelling induced changes in near bottom density gradients. Mesoscale eddies are also shown to develop both shelf-depth and continental slope INLs [*Washburn et al.*, 1993; *McCave et al.*, 2001]. Although INL signals caught by nephelometers and transmissometers are mainly due to fine particles, *McCave et al.* [2001] explain offshore increase in trapped sediment flux with depth in their study on the European

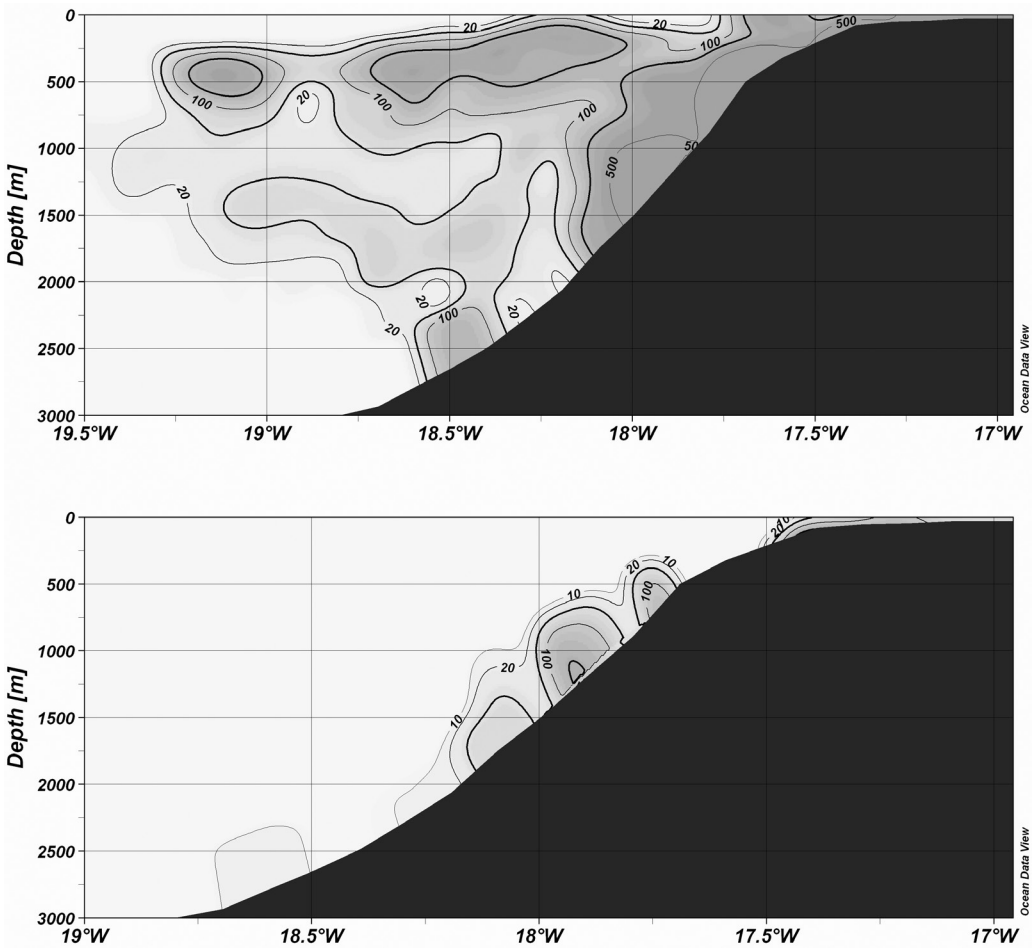

Figure 8. Cross shore distribution of Class A particles (top) and downslope migration of Class B particles (bottom) along the zonal transect 21.2°N off Cape Blanc on simulation day 1035 (concentrations in relative units).

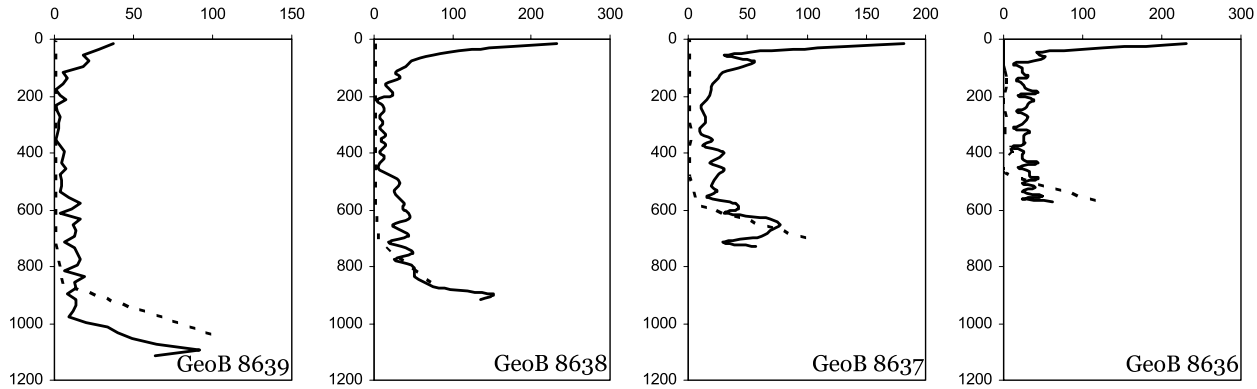

Figure 9. Vertical profiles of Class B particles (1-month averaged, dashed lines, in relative units) against observed particle profiles (black lines, in number per liter) during cruise M58-2B at the cross-shore located profiling stations GeoB 8636 through 8639 (positions are shown in Figure 1).

margin at 47°–50°N by suggesting that large particles are also carried in INLs. It can be argued that in Cape Blanc region, vigorous upwelling year round and the mesoscale dynamics along with turbulent mixing processes produced by the confluence of two water masses of different origin prepare the optimal physical conditions for INL production.

[38] In our simulations the main property of the particles that determines the extent of their vertical and lateral transport in the system is their sinking velocities. Good agreement with particle camera data is achieved with a relatively small sinking velocities of 5 m day^{-1}, while simulations with larger sinking rates result in too deep particle maxima and a too rapid offshore particle concentration decrease. In fact, a variety of settling velocity formulas developed for spherical particles and natural sediments [*Jimenez and Madsen*, 2003] gives much smaller particle diameters for the sinking velocities of both particle classes that we have used in the shelf erosion experiment than those that can be measured by the particle camera employed by Nowald et al. (submitted manuscript, 2006). However, marine particulate matter sinks to deeper layers in the form of aggregates, which usually have smaller settling velocities than idealized spherical particles. We therefore argue that the particles observed in the camera profiles and transported offshore from the shelf in the numerical experiments are aggregates. In their study on the western European continental margin, *Thomsen and Gust* [2000] present evidence for this argument. The authors report a two-layer concept of sediment interface, where a layer of cohesive sediments underlies a more easily resuspendable surface aggregate layer. They show a negative correlation between the aggregate size and erosion resistance and suggest that these aggregates are transported over long distances since their settling velocities are smaller than those of similar-size sand particles.

[39] Various sinking velocities for aggregates have been reported in the literature. Although *Alldredge and Gotschalk* [1988] demonstrate an exponential relation between sinking rate and aggregate size and report fast sinking velocities, *Asper* [1987] and *Diercks and Asper* [1997] find no correlation between the settling velocity and size of aggregates and give an account of a wide range of settling velocities, even in the same size classes. Similarly, *Shanks* [2002] measured rather diverse rates of sinking velocities in Cape Lookout Bight. *Azetsu-Scott and Passow* [2004] indicate the significance of transparent exopolymer particles (TEP) in forming aggregates of all sizes with solid particles. They show that particle-free TEP, which is contained in marine aggregates, is positively buoyant and depending on the volume fractions of solid matter, TEP, and interstitial water in natural marine snow-sized aggregates, it can regulate the export flux of particulate matters by influencing the settling velocity. In another study, *Engel and Schartau* [1999] report that as the TEP content of an aggregate increases, the sinking velocity falls and the size versus velocity relationship becomes less pronounced. Besides, *Kiørboe et al.* [1998] observed low levels of particle flux during the diatom bloom despite intensive aggregate formation in St Helena Bay on the west coast of South Africa. The aggregates were nearly neutrally buoyant and no increase was seen in aggregate size with depth, which implies that sinking velocity of aggregates does not necessarily depend on their size. Therefore there exists substantial evidence that the sinking velocity of 5 m day^{-1} is not unrealistic for those particles observed in the camera profiles, which makes their transport from shelf to open ocean in subsurface layers possible.

[40] Particles caught in sediment traps in the region typically have sinking velocities between 100 and 200 m day^{-1} [*Wefer and Fischer*, 1993]. At these sinking speeds the particles reside in the upper water column for only a few days, and lateral translation due to ocean currents is limited [*Siegel and Deuser*, 1997]. While being responsible for a great part of the vertical material flux, due to their large sinking velocity and mass, the concentration of these particles in the water column is low and they contribute little to the particle abundance measured by the particle cameras.

5. Conclusions

[41] Employing an ocean model with sediment transport and ecosystem modules in a high resolution and nested configuration, numerical experiments were conducted to locate the source of surface and subsurface particle maxima detected by particle camera profiler during recent cruises in

the Cape Blanc region. It is shown that the surface maxima is generated by the local primary production. In contrast, erosion of particulate matter from the shelf gives rise to pronounced subsurface particle plumes and appear to be the most likely source of the observed middepth particle maxima. Persistent upwelling creates favorable conditions for the offshore transport and dispersion of particles in a pulse-like and patchy pattern with the involvement of eddies and filaments at various temporal and spatial scales. Relatively heavy particles, on the other hand, migrate downslope along the ocean floor and are conveyed from the shelf edge to the continental slope. Effective transport distance of particles indicates that between 20.5°N and 23.5°N the offshore transport is the most intense, due to vigorous turbulent mixing processes resulted from the confluence of different water masses off Cape Blanc.

[42] **Acknowledgments.** We would like to thank two anonymous reviewers for their helpful suggestions. Numerical experiments were carried out on IBM pSeries 690 Supercomputer of Norddeutscher Verbund für Hoch- und Höchstleistungsrechnen (HLRN). This research was funded by the Deutsche Forschungsgemeinschaft – Research Center Ocean Margins at the University of Bremen (RCOM0361).

References

Alldredge, A. L., and C. Gotschalk (1988), In situ settling behaviour of marine snow, *Limnol. Oceanogr.*, *33*, 339–351.

Arístegui, J., et al. (1997), The influence of island-generated eddies on chlorophyll distribution: A study of mesoscale variation around Gran Canaria, *Deep Sea Res., Part I*, *44*, 71–96.

Arístegui, J., E. D. Barton, P. Tett, M. F. Montero, M. García-Muñoz, G. Basterretxea, A. Cussatlegras, A. Ojeda, and D. de Armas (2004), Variability in plankton community structure, metabolism, and vertical carbon fluxes along an upwelling filament (Cape Juby, NW Africa), *Progr. Oceanogr.*, *62*, 95–113.

Armstrong, R. A., C. Lee, J. I. Hedges, S. Honjo, and S. G. Wakeham (2002), A new, mechanistic model for organic carbon fluxes in the ocean based on the quantitative association of POC with ballast minerals, *Deep Sea Res., Part II*, *49*, 219–236.

Asper, V. (1987), Measuring the flux and sinking speed of marine snow aggregates, *Deep Sea Res.*, *34*, 1–17.

Azetsu-Scott, K., and U. Passow (2004), Ascending marine particles: Significance of transparent exopolymer particles (TEP) in the upper ocean, *Limnol. Oceanogr.*, *49*, 741–748.

Barton, E. D. (1987), Meanders, eddies and intrusions in the thermohaline front off Northwest Africa, *Oceanol. Acta*, *10*(3), 267–283.

Barton, E. D. (1998), Eastern boundary of the North Atlantic: Northwest Africa and Iberia, in *The Sea*, edited by A. R. Robinson and K. H. Brink, pp. 633–657, John Wiley, Hoboken, N. J.

Barton, E. D., et al. (1998), The transition zone of the Canary Current upwelling region, *Prog. Oceanogr.*, *41*, 455–504.

Bauer, J. E., and E. R. M. Druffel (1998), Ocean margins as a significant source of organic matter to the deep ocean, *Nature*, *392*, 482–485.

Behrenfeld, M. J., and P. G. Falkowski (1997), Photosynthetic rates derived from satellite-based chlorophyll concentration, *Limnol. Oceanogr.*, *42*, 1–20.

Blaas, M., C. Dong, P. Marchesiello, J. C. McWilliams, and K. D. Stolzenbach (2006), Sediment transport modeling on Southern Californian shelves: A ROMS case study, *Cont. Shelf Res.*, in press.

Blayo, E., and L. Debreu (1999), Adaptive mesh refinement for finite-difference ocean models: First experiments, *J. Phys. Oceanogr.*, *29*(6), 1239–1250.

Boyer, T. P., C. Stephens, J. I. Antonov, M. E. Conkright, R. A. Locarnini, T. D. O'Brian, and H. E. Garcia (2002), *World Ocean Atlas 2001*, vol. 1, *Salinity*, *NOAA Atlas NESDIS 50*, edited by S. Levitus, 165 pp., U.S. Govt. Print. Off., Washington, D. C.

Bricaud, A., A. Morel, and J. M. André (1987), Spatial/temporal variability of algal biomass and potential productivity in the Mauritanian upwelling zone, as estimated from CZCS data, *Adv. Space Res.*, *7*, 53–62.

Chassignet, E. P., and P. Malanotte-Rizzoli (2000), Ocean circulation model evaluation experiments for the North Atlantic basin, *Dyn. Atmos. Oceans*, *32*, 155–432.

Chassignet, E. P., H. Arango, D. Dietrich, T. Ezer, M. Ghil, D. B. Haidvogel, C. C. Ma, A. Mehra, A. M. Paiva, and Z. Sirkes (2000), DAMÉE-NAB: The base experiments, *Dyn. Atmos. Oceans*, *32*, 155–183.

Davenport, R., S. Neuer, A. Hernandez-Guerra, M. J. Rueda, O. Llinas, G. Fischer, and G. Wefer (1999), Seasonal and interannual pigment concentration in the Canary Islands region from CZCS data and comparison with observations from the ESTOC, *Int. J. Remote Sens.*, *20*(7), 1419–1433.

Davenport, R., S. Neuer, P. Helmke, J. Perez-Marrero, and O. Llinas (2002), Primary productivity in the northern Canary Islands region as inferred from SeaWiFS imagery, *Deep Sea Res., Part II*, *49*, 3481–3496.

De Haas, H., T. C. E. Van Weering, and H. De Stieger (2002), Organic carbon in shelf seas: Sinks or sources, processes and products, *Cont. Shelf Res.*, *22*, 691–717.

Dickson, R. R., and I. N. McCave (1986), Nepheloid layers on the continental slope west of Porcupine Bank, *Deep Sea Res., Part A*, *33*, 791–818.

Diercks, A. R., and V. Asper (1997), In situ settling speeds of marine snow aggregates below the mixed layer: Black Sea and Gulf of Mexico, *Deep Sea Res., Part I*, *44*, 385–398.

Dupouy, C., and H. Demarcq (1987), CZCS as an aid for understanding modalities of the phytoplankton productivity during upwelling off Senegal, *Adv. Space Res.*, *7*, 63–71.

Engel, A., and M. Schartau (1999), Influence of transparent exopolymer particles (TEP) on sinking velocity of Nitzschia closterium aggregates, *Mar. Ecol Progr. Ser.*, *182*, 69–76.

Fasham, M. J. R., H. W. Ducklow, and S. M. McKelvie (1990), A nitrogen-based model of plankton dynamics in the oceanic mixed layer, *J. Mar. Res.*, *48*, 591–639.

Frignani, M., T. Courp, J. K. Cochran, D. Hirschberg, and L. V. I. Codina (2002), Scavenging rates and particle characteristics in and near the Lacaze-Duthiers submarine canyon, northwest Mediterranean, *Cont. Shelf Res.*, *22*, 2175–2190.

Fütterer, D. (1983), The modern upwelling record off northwest Africa, in *Coastal Upwelling, its Sediment Record, Part B: Sedimentary Records of Ancient Coastal Upwelling*, edited by J. Thiede and E. Suess, pp. 105–121, Plenum, New York.

Gabric, A. J., L. Garcia, L. Van Camp, L. Nykjaer, W. Eifler, and W. Schrimpf (1993), Offshore Export of Shelf Production in the Cape Blanc (Mauritania) Giant Filament as Derived From Coastal Zone Color Scanner Imagery, *J. Geophys. Res.*, *98*(C3), 4697–4712.

García-Muñoz, M., J. Arístegui, M. F. Montero, and E. D. Barton (2004), Distribution and transport of organic matter along a filament-eddy system in the Canaries – NW Africa coastal transition zone region, *Progr. Oceanogr.*, *62*, 115–129.

García-Muñoz, M., J. Arístegui, J. L. Pelegrí, A. Antoranz, A. Ojeda, and M. Torres (2005), Exchange of carbon by an upwelling filament off Cape Ghir (NW Africa), *J. Mar. Syst.*, *54*, 83–95.

Haidvogel, D. B., and A. Beckmann (1999), *Numerical Ocean Circulation Modeling*, 330 pp., Imperial College Press, London.

Haidvogel, D. B., H. G. Arango, K. Hedstrom, A. Beckmann, P. Malanotte-Rizzoli, and A. F. Shchepetkin (2000), Model evaluation experiments in the North Atlantic Basin: Simulations in nonlinear terrain-following coordinates, *Dyn. Atmos. Oceans*, *32*(3–4), 239–281.

Hall, I. R., S. Schmidt, I. N. McCave, and J. L. Reyss (2000), Particulate matter distribution and $^{234}Th/^{238}U$ disequilibrium along the Northern Iberian Margin: Implications for particulate organic carbon export, *Deep Sea Res., Part I*, *47*, 557–582.

Hernández-Guerra, A., J. Arístegui, M. Canton, and L. Nykjær (1993), Phytoplankton pigment patterns in the Canary Islands as determined using Coastal Zone Colour Scanner data, *Int. J. Remote Sens.*, *14*, 1431–1437.

Jahnke, R. A. (1996), The global ocean flux of particulate organic carbon: Areal distribution and magnitude, *Global Biogeochem. Cycles*, *10*, 71–88.

Jickells, T. D., et al. (2005), Global iron connections between desert dust, ocean biogeochemistry, and climate, *Science*, *308*, 67–71.

Jimenez, J. A., and O. S. Madsen (2003), A simple formula to estimate settling velocity of natural sediments, *J. Water. Port C-ASCE*, *129*(2), 70–78.

Kiørboe, T., P. Tiselius, B. Mitchell-Innes, J. L. S. Hansen, A. W. Visser, and X. Mari (1998), Intensive aggregate formation with low vertical flux during an upwelling-induced diatom bloom, *Limnol. Oceanogr.*, *43*, 104–116.

Kostianoy, A. G., and A. G. Zatsepin (1996), The West African coastal upwelling filaments and cross-frontal water exchange conditioned by them, *J. Mar. Syst.*, *7*, 349–359.

Lange, C. B., O. E. Romero, G. Wefer, and A. J. Gabric (1998), Offshore influence of coastal upwelling off Mauritania, NW Africa, as recorded by diatoms in sediment traps at 2195 m water depth, *Deep Sea Res., Part I*, *45*, 985–1013.

Large, W. G., J. C. McWilliams, and S. Doney (1994), Oceanic vertical mixing: A review and a model with a nonlocal boundary layer parameterization, *Rev. Geophys.*, *32*(4), 363–404.

Mahowald, N., K. Kohfeld, M. Hansson, Y. Balkanski, S. P. Harrison, I. C. Prentice, M. Schulz, and H. Rodhe (1999), Dust sources and deposition during the last glacial maximum and current climate: A comparison of model results with paleodata from ice cores and marine sediments, *J. Geophys. Res.*, *104*, 15,895–15,916.

Marchesiello, P., J. C. McWilliams, and A. Shchepetkin (2001), Open boundary conditions for long-term integration of regional oceanic models, *Ocean Model.*, *3*, 1–20.

Marchesiello, P., J. C. McWilliams, and A. Shchepetkin (2003), Equilibrium structure and dynamics of the California Current System, *J. Phys. Oceanogr.*, *33*, 753–783.

Marchesiello, P., S. Herbette, L. Nykjaer, and C. Roy (2004), Eddy-driven dispersion processes in the Canary Current upwelling system: Comparison with the California system, *Globec Int. Newsl.*, *10*, 5–7.

McCave, I. N., I. R. Hall, A. N. Antia, L. Chou, F. Dehairs, R. S. Lampitt, L. Thomsen, T. C. E. van Weering, and R. Wollast (2001), Distribution, composition and flux of particulate material over the European margin at 47°–50°N, *Deep Sea Res., Part II*, *48*, 3107–3139.

McPhee-Shaw, E. E., R. W. Sternberg, B. Mullenbach, and A. S. Ogston (2004), Observations of intermediate nepheloid layers on the northern California continental margin, *Cont. Shelf Res.*, *24*, 693–720.

Meincke, J., C. LeProvost, and J. Willebrand (2001), Dynamics of the North Atlantic circulation (DYNAMO), *Prog. Oceanogr.*, *48* (2–3), 335 pp.

Mittelstaedt, E. (1991), The ocean boundary along the northwest African coast: Circulation and oceanographic properties at the sea surface, *Prog. Oceanogr.*, *26*, 307–355.

Muller-Karger, F. E., R. Varela, R. Thunell, R. Luerssen, C. Hu, and J. J. Walsh (2005), The importance of continental margins in the global carbon cycle, *Geophys. Res. Lett.*, *32*, L01602, doi:10.1029/2004GL021346.

Neuer, S., T. Freudenthal, R. Davenport, O. Llinás, and M. Rueda (2002), Seasonality of surface water properties and particle flux along a productivity gradient off NW Africa, *Deep Sea Res., Part II*, *49*, 3561–3576.

Nykjær, L., and L. Van Camp (1994), Seasonal and interannual variability of coastal upwelling along northwest Africa and Portugal from 1981 to 1991, *J. Geophys. Res.*, *99*, 14,197–14,207.

Paropkari, A. L., C. P. Babu, and A. Mascarenhas (1992), A critical evaluation of depositional parameters controlling the variability of organic carbon in Arabian Sea sediments, *Mar. Geol.*, *107*, 213–220.

Pelegrí, J. L., J. Arístegui, L. Cana, M. González-Dávila, A. Hernández-Guerra, S. Hernández-León, A. Marrero-Díaz, M. F. Montero, P. Sangrà, and M. Santana-Casiano (2005), Coupling between the open ocean and the coastal upwelling region off northwest Africa: Water recirculation and offshore pumping of organic matter, *J. Mar. Syst.*, *54*, 3–37.

Penven, P., L. Debreu, P. Marchesiello, and J. C. McWilliams (2006), Application of he ROMS embedding procedure in the California Current System, *Ocean Model.*, *12*, 157–187.

Ratmeyer, V., G. Fischer, and G. Wefer (1999), Lithogenic particle fluxesand grain size distributions in the deep ocean off northwest Africa: Implications for seasonal changes of aeolian dust input and downward transport, *Deep Sea Res., Part I*, *46*, 1289–1337.

Richardson, P. L., S. Arnault, S. Garzoli, and J. G. Bruce (1992), Annual cycle of the Atlantic North Equatorial Countercurrent, *Deep Sea Res., Part A*, *39*, 997–1014.

Schlitzer, R. (2000), Applying the adjoint method for biogeochemical modeling: Export of particulate organic matter in the world ocean, in *Inverse Methods in Global Biogeochemical Cycles*, *Geophys. Monogr. Ser.*, vol. 114, edited by P. Kasibhata, pp. 107–124, AGU, Washington, D. C.

Shanks, A. (2002), The abundance, vertical flux, and still-water and apparent sinking rates of marine snow in a shallow coastal water column, *Cont. Shelf Res.*, *22*, 2045–2064.

Shchepetkin, A. F., and J. C. McWilliams (1998), Quasi-monotone advection schemes based on explicit locally adaptive disspiation, *Mon. Weather Rev.*, *126*, 1541–1580.

Shchepetkin, A. F., and J. C. McWilliams (2003), A method for computing horizontal pressure-gradient force in an oceanic model with a nonaligned vertical coordinate, *J. Geophys. Res.*, *108*(C3), 3090, doi:10.1029/2001JC001047.

Shchepetkin, A., and J. C. McWilliams (2005), The Regional Oceanic Modeling System: A split-explicit, free-surface, topography-following-coordinate ocean model, *Ocean Model.*, *9*, 347–404.

Siegel, D. A., and W. G. Deuser (1997), Trajectories of sinking particles in the Sargasso Sea: Modeling of statistical funnels above deep-ocean sediment traps, *Deep Sea Res., Part I*, *44*, 1519–1541.

Silva, A., C. Young, and S. Levitus (1994), *Atlas of Surface Marine Data 1994*, vols. 1–5, *NOAA Atlas NESDIS 6–10*, U.S. Govt. Print. Off., Washington, D. C.

Smith, W. H. F., and D. T. Sandwell (1997), Global seafloor topography from satellite altimetry and ship depth soundings, *Science*, *277*, 1957–1962.

Stephens, C., J. I. Antonov, T. P. Boyer, M. E. Conkright, R. A. Locarnini, T. D. O'Brian, and H. E. Garcia (2002), *World Ocean Atlas 2001*, vol. 1, *Temperature*, *NOAA Atlas NESDIS 49*, edited by S. Levitus, 167 pp., U.S. Govt. Print. Off., Washington, D. C.

Stramma, L., and F. Schott (1999), The mean flow field of the tropical Atlantic Ocean, *Deep Sea Res., Part I*, *46*, 279–303.

Thomsen, L., and G. Gust (2000), Sediment erosion thresholds and characteristics of resuspended aggregates on the western European continental margin, *Deep Sea Res., Part I*, *47*, 1881–1897.

Thomsen, L., and T. van Weering (1998), Spatial and temporal variability of particulate matter in the benthic boundary layer at the NW European Continental Margin (Goban Spur), *Progr. Oceanogr.*, *42*, 61–76.

Thomsen, L., T. van Weering, and G. Gust (2002), Processes in the benthic boundary layer at the Iberian continental margin and their implication for carbon mineralization, *Progr. Oceanogr.*, *52*, 315–329.

Van Camp, L., L. Nykjær, E. Mittelstaedt, and P. Schlittenhardt (1991), Upwelling and boundary circulation off northwest Africa as depicted by infrared and visible satellite observations, *Prog. Oceanogr.*, *26*, 357–402.

van Weering, T. C. E., W. Helder, and P. Schalk (1997), The Netherlands Indian Ocean expedition 1992–1993, first results and an introduction, *Deep Sea Res., Part II*, *44*, 1177–1193.

van Weering, T. C. E., H. C. de Stigter, W. Boer, and H. de Haas (2002), Recent sediment transport and accumulation on the NW Iberian margin, *Progr. Oceanogr.*, *52*, 349–371.

Washburn, L., M. S. Svenson, J. L. Largier, P. M. Kosro, and S. R. Ramp (1993), Cross-shelf sediment transport by an anticyclonic eddy off northern California, *Science*, *26*, 1560–1564.

Wefer, G., and G. Fischer (1993), Seasonal patterns of vertical particle flux in equatorial and coastal upwelling areas of the eastern Atlantic, *Deep Sea Res., Part I*, *40*, 1613–1645.

Wheatcroft, R. A., C. K. Sommerfield, D. E. Drake, J. C. Borgeld, and C. A. Nittrouer (1997), Rapid and widespread dispersal of flood sediment on the northern California margin, *Geology*, *25*, 163–166.

Wooster, W. S., and J. L. Reid (1963), Eastern boundary currents, in *The Sea II*, edited by M. N. Hill, pp. 253–280, Interscience, Hoboken, N. J.

M. Blaas, WL|Delft Hydraulics, P. O. Box 177, N-2600 MH Delft, Netherlands.

S. Frickenhaus, G. Karakaş, and R. Schlitzer, Alfred Wegener Institute for Polar and Marine Research, Columbusstrasse, D-27568 Bremerhaven, Germany. (gkarakas@awi-bremerhaven.de)

P. Marchesiello, Institut de Recherche pour le Développement, B. P. 70, F-29280 Plouzane, France.

N. Nowald, Department of Geosciences, University of Bremen, Klagenfurterstrasse, D-28359 Bremen, Germany.